Journal of Hazardous Materials 169 (2009) 386–394

Contents lists available at ScienceDirect

Journal of Hazardous Materials

journal homepage: www.elsevier.com/locate/jhazmat

Activation of Firmiana Simplex leaf and the enhanced Pb(II) adsorption performance: Equilibrium and kinetic studies

Zhenze Li, Xiaowu Tang*, Yunmin Chen, Liming Wei, Yan Wang

MOE Key Laboratory of Soft Soils and Geoenvironmental Engineering, Department of Civil Engineering, Zhejiang University, Yuhangtang Rd. 388, Hangzhou, 310058, PR China

ARTICLE INFO

Article history:
Received 14 October 2008
Received in revised form 23 March 2009
Accepted 24 March 2009
Available online 31 March 2009

Keywords:
Firmiana Simplex leaf
Activated leaf
Pb(II)
Adsorption
Phosphate

ABSTRACT

Although various biosorbents have been reported effective to purify wastewaters containing heavy metals, the high tendency to decomposition in the environment makes them unsuitable for long-term persistent utilization. In this paper, a simple and new activation method was proposed to mineralize the Firmiana Simplex leaf (FSL) into an enhanced adsorbent for Pb(II) removal from aqueous solution. The leaves activated at various temperatures were characterized with BET N_2 adsorption test, FT-IR test and XRD test. After activation, the mass percent of inorganic components (including whewellite, quartz, phosphate and calcite) increased and the specific surface area increased from 0.08283 to 9.32 $m^2\,g^{-1}$ with the increasing activation temperature (AT) from 100 to 400 °C. Proper activation temperature (200 °C) helps to preserve the beneficial groups (amine and carboxyl). The affinities of the adsorbents towards Pb(II) were increased with increasing AT from 300, 100, 200 to 400 °C according to the adsorption isotherms. The adsorbent activated at 200 °C (AL2) was found most suitable for Pb(II) adsorption regarding the high yield efficiency (36.52%), high Pb(II) adsorption capacity (136.7 mg g^{-1} by Langmuir model), high adsorption affinity (H type isotherm) and rapid adsorption rate (within 20 min by kinetic study). The Pb(II) removal efficiency of AL2 was obviously affected by the solution pH rather than by the adsorbent dosage. The adsorption was viewed as a chemical process based on IR spectra along with a physical process based on the correlation between the average pore size of the adsorbent and the adsorption capacity. The activation method proposed in this paper was proved effective and potentially applicable in the treatment of Pb(II) polluted wastewaters.

1. Introduction

Lead is toxicant to living things and has been strictly legislated in drinking water in many countries [1]. The lead concentration is reported very high in acid mining drainages from lead zinc mining sites [2,3]. In developing countries, the uncontrolled discharge of lead contaminated wastewater has caused serious health problems as well as potential threats to the long-term sustainable development of the local economy [2,3]. It is stringent to develop efficient and cost-effective treatment methods based on the local situations. Although many methods are applicable for wastewater treatment, the adsorption method seems as one of the most prominent choice [4–11].

Firmiana Simplex tree is widely planted throughout China. In deep autumn, the fallen leaf covers the land surface (several inches depth) and always imposes great burden on the street sweeping. The fallen leaf could be landfilled, incinerated or incubated [12]. Because of the large production and low combustion energy of the fallen leaf, the limited capacity of landfills and harmful emissions by incinerations, it is necessary to develop new treatment methods.

In China, lead zinc mining sites are always located in mountain areas in southern China where the humid and warm climate results in luxuriant vegetations. One cost-effective method to remove heavy metals from the wastewaters is to make the locally available leaves into utilizable biosorbents. Biosorption of heavy metals with natural products has been widely reported [4–11,13]. Firmiana Simplex leaf (FSL) shows satisfactory performance in dyes adsorption from discharged wastewaters [14]. But the long-term biodegradation of these natural adsorbents limits the practical application.

Activated carbon made from leaf by calcination under nitrogen atmosphere was reported with large adsorption capacity with respect to the relevant structure and morphology [15]. However, the high energy and nitrogen consumption significantly increase the preparation cost and thus make it too expensive to apply in practice. In this paper, the authors attempted to develop a method (i) to reach the similar target of making leaf into activated carbon under relatively common conditions; (ii) to mineralize the natural organics to prevent possible natural decomposition; (iii) to pertain certain part of beneficial functional groups of crude leaf to enhance the adsorption behavior.

* Corresponding author. Tel.: +86 571 88208791; fax: +86 571 85023966.
E-mail address: tangxiaowu@zju.edu.cn (X. Tang).

0304-3894/$ – see front matter © 2009 Elsevier B.V. All rights reserved.
doi:10.1016/j.jhazmat.2009.03.108

From this perspective, a simple and new method was developed to activate FSL by calcination at specific temperatures in the presence of limited oxygen. The adsorption behavior of Pb(II) on the obtained adsorbents (activated leaf, AL in short) and the relevant affecting factors were investigated using Batch method. N_2 adsorption test was carried out to evaluate the change in the surface properties of various adsorbents. FT-IR patterns and XRD spectra were used to explain the mechanism of the activation of natural leaf and the adsorption of Pb(II).

2. Materials and methods

The FSL was collected from fallen leaves in the campus of Zhejiang University in October, 2007. There was no visually observed ash on the leaf surface due to the good air quality in the city. The collected leaf was oven dried at 45 °C overnight and then pulverized to pass 24 mesh screen with diameters 355 ±13 μm. The powder was stored in plastic bags for further tests. Stock solution of lead nitrate in analytical grade was prepared and diluted to target concentration for further tests. Conical flasks and centrifuging tubes were immersed in 0.01 M HNO_3 solution overnight and then rinsed 3 times with de-ionized water.

2.1. Preparation of the adsorbent

The leaf was weighed (350 g) and placed on a ceramic plate which was then transferred into an oven (15 cm × 25 cm × 40 cm). The door of the oven was closed and sealed except that a small hole (0.5 cm diameter) was left open to release the possible air emission. The temperature was increased from room temperature to 100, 200, 300, and 400 °C (the activated leaf shorten as AL1, AL2, AL3 and AL4 accordingly), separately with an increment of 25–30 °C/min, and then pertained for 5 h. There was no gas supply into the oven during the calcination process. Once the treatment duration was reached, the power of the oven was shut off and the product was allowed to cool to room temperature. The obtained ashes were collected, weighed and stored in sealed plastic bags.

2.2. Characterization

Natural pHs (pH_{na}) of various ALs were measured by glass electrode potentiometer following the method used by previous works [16]. BET N_2 adsorption test was conducted to determine the specific surface area (SSA) of the crude leaf and the activated adsorbents using Autosorb 1-MP apparatus (Quantachrome Corporation, USA). The test results were analyzed using BET adsorption theory to predict the relevant parameters for each adsorbent.

FT-IR spectra of various activated leaf were recorded using Nexus-670 (Nicolet, USA) to study the changes in the functional groups. The sample was dried under infrared radiation for 10 min, ground into fine powder with KBr in a carnelian mortar, compressed into a translucent slice under 40 MPa and then exposed to infrared radiation to determine the functional groups. The XRD spectra of ALs were investigated with D/MAX-RA (Rigaku Corp., Japan, equipped with a Cu Kα tube and Ni filter) apparatus. The samples were dried by infrared radiation and then pulverized and subjected to X-ray radiation.

The FT-IR spectra of Pb(II) laden adsorbents (AL2) were obtained to investigate the mechanism of Pb(II) adsorption. Solutions with increasing initial Pb(II) concentration from 10 to 20, 40 and 80 mg L^{-1} were equilibrated with the adsorbent (0.1 g/50 mL), respectively, for 24 h in order to prepare the Pb(II) laden adsorbents. The samples were treated following the above-mentioned processes.

2.3. Experiments

2.3.1. Isothermal adsorption of Pb(II) on ALs

The AL (0.100 ± 0.002 g) was sampled and placed in glass conical flask. Pb(II) solution (50 mL) with increasing solute concentration from 10 to 900 mg L^{-1} was then poured into the flask. The mixture was equilibrated in agitator at 25 °C, 180 rpm for 24 h. After that, the slurry was poured to a centrifuge tube and then centrifuged at 3000 rpm for 5 min. The Pb(II) concentration of the supernatant was determined by Atomic Absorption Spectroscopy (AAS) with Hitachi 180-80 apparatus (Japan). The duplicates and blanks were conducted.

Four ALs (calcinated at 100, 200, 300 and 400 °C, separately), were separately subjected to Pb(II) adsorption using the aforementioned Batch method. The adsorption amount was obtained by subtracting the initial solute amount (concentration × volume, $C_0 \times V$) by the equilibrium concentration (concentration × volume, $C_e \times V$) and the quantity of Pb(II) adsorbed on the flask (from blank test).

Judged by the yield efficiency (mass ratio of the activated leaf to the original dry leaf), energy consumption and the Pb(II) adsorption isotherm of each adsorbent, AL2 was found superior to others and was chosen as the potential adsorbent for further study.

2.3.2. Effect of adsorbent dosage

Pb(II) solution (50 mg L^{-1}, 50 mL) was prepared and transferred to conical flask (250 mL). The adsorbent, AL2, was weighed and mixed with the solution. The dosage was ranged from 0.025 to 0.30 g per 50 mL. All flasks were placed on an agitator at constant temperature 25 °C, 180 rpm for 24 h. The slurry was centrifuged at the end of the test and the Pb(II) concentration in the supernatant was determined by AAS. Blanks and duplicates were also carried out.

2.3.3. Effect of pH

Pb(II) solution (65 mg L^{-1}, 50 mL) was mixed with AL2 (0.100 ± 0.002 g) and agitated at 180 rpm, 25 °C for 24 h. The solution pH was previously adjusted to increased pH_i from 2.0 to 7.8 with 0.001–0.1 M HNO_3 or NaOH solution. The mixture was centrifuged at 3000 rpm for 5 min to separate. The supernatant was collected and the equilibrium concentration of Pb(II) was determined by AAS. The equilibrium pH of the solution was determined using a glass electrode (Shanghai Precision & Scientific Instrument Co., China). Batch adsorption test was conducted following the similar processes to the above tests.

2.3.4. Adsorption kinetics

Three aliquots of Pb(II) solution (50 mL) were mixed with AL2 (0.100 ± 0.002 g) in three conical flasks with 50, 100 and 200 mg L^{-1} Pb(II), separately. The mixture was agitated at 180 rpm, 25 °C. The equilibration of the three sets of sample was stopped at different reaction time ranging from 10 to 205 min. The slurry was quickly poured into centrifuging tube to separate at 3000 rpm for 5 min. The equilibrium Pb(II) concentration of the supernatant was determined by AAS. Blanks and duplicates were both conducted.

2.3.5. Recycling of waste adsorbent

The AL2 (0.100 ± 0.002 g) was firstly equilibrated with Pb(II) (50 mL, 50 mg L^{-1}) overnight and then get separated by centrifuging at 3000 rpm for 5 min. The Pb(II) concentration of the supernatant was determined by AAS. The solid residual was further mixed with 50 mL 0.01 M HNO_3, 0.01 M EDTA, 0.01 M NH_4Cl, and 0.01 M citric acid solutions, separately. The mixtures were agitated overnight following the same method to Batch adsorption test. The obtained slurry was centrifuged and the Pb(II) concentration in the supernatant was determined by AAS. Blanks and duplicates were both conducted.

Table 1
Yield efficiencies, natural pHs and surficial parameters of various ALs.

Sample	Activation temperature °C	Yield efficiencies	pH_{na}	Specific surface area ($m^2\ g^{-1}$)	Total pore volume ($m^2\ g^{-1}$)	Average pore size (Å)	Correlation coefficient (R^2)
AL1	100	90.31%	6.60	0.08283	NA	NA	0.8717
AL2	200	36.52%	8.63	1.619	0.02498	617.3	0.7077
AL3	300	21.21%	10.36	4.639	0.02881	248.4	0.9587
AL4	400	15.26%	10.92	9.320	0.1894	813.0	0.7582

3. Results and discussions

3.1. Characterization of the ALs

Table 1 shows the yield efficiency of the four ALs at different activation temperatures. The yield efficiency was decreased from 90.31 to 36.52, 21.21 and 15.26% with increasing ATs from 100 to 200, 300 and 400 °C, respectively. About 10% weight loss (reduction of the weight of natural dry leaf after treatment at higher temperatures) of the natural dry leaf was observed at 100 °C, which could be attributed to a physical process (the volatile low molecule organics would be evaporated) rather than a chemical reaction caused by ignition. Higher activation temperature (AT) will result in increased degree of degradation and activation. The weight loss of AL2 (63.48%) was comparatively lower than those of AL2 (78.79%) and AL3 (84.74%) prepared at higher temperatures.

The natural pHs of the four kinds of ALs were determined at 6.60, 8.63, 10.36 and 10.92 for AL1, AL2, AL3 and AL4, separately, as shown in Table 1. ATs higher than 200 °C will form alkaline composition which could give rise to the natural pHs of ALs.

Table 1 also shows the results of N_2 adsorption test analyzed by BET adsorption theory. The SSA was observed increasing from 0.08283 to 1.619, 4.639 and 9.320 $m^2\ g^{-1}$ with increasing AT from 100 to 200, 300 and 400 °C, separately. A 112.5 times increase in SSA of natural leaf was achieved after activated at 400 °C. The total pore volumes of AL2, AL3 and AL4 were determined at 0.02498, 0.02881 and 0.1894 $mL\ g^{-1}$, separately. The average pore sizes of the activated adsorbents were in the sequence of AL4 > AL2 > AL3 while the largest was about 2.3 times higher than the least. The total pore volume and average pore size were not available for AL1.

AL4 seems as the best choice for heavy metal adsorption in view of the SSA, total pore volume and average pore size that are directly related to the adsorption performance. AL2 although, has comparatively lower SSA than AL3, has similar total pore volume and even 1.48-fold higher average pore size than the latter. Therefore, AL2 seems more preponderant than AL3 with respect to the obviously less energy consumption of AL2 than that of AL3.

3.1.1. IR spectra of various ALs

Fig. 1a shows the FT-IR spectra of the four ALs. In general, the relevant functional groups on the ALs could be determined based on the FT-IR adsorption band (Table 2). AL1 represents the major property of natural FSL because the organism has not changed at this temperature. The relevant proportions of the functional groups in AL1 could be sequenced, due to the band intensities, as: NH > COH > OH > CH > C=O ≫ C–O–C > SiO > POH. As to AL2, the main functional groups could be determined and sequenced as: NH > C=O > OH > SiO > POH > CH > CN > O=C–N. The functional

Table 2
Band position in the FT-IR spectra of ALs.

Sample				Assignment	Reference
AL1	AL2	AL3	AL4		
3415 (vs)	3425 (vs)	3423 (vs)	3426 (vs)	OH stretching	[17]
	3340 (m)	3344 (s)		Free OH bending	
	3270 (m)	3268 (s)		Free OH bending	
	3064 (m)	3066 (s)		Aromatic C–H stretching	[17]
2922 (s)	2929 (w)	2931 (w)		C–H	
2852 (s)	2852 (w)			C–H	
			2516 (m)	P–O–H asymmetric stretching/C=O	[18]
			2364 (m)	P–O–H bending	
			2345 (m)	P–O–H bending/C=O	
1793 (vw)			1797 (m)	C=O	
1737 (m)				C=O	
1631 (vs)				N–H	
1623 (vs)	1619 (vs)	1618 (vs)	1618 (vs)	N–H	
1457 (vw)		1438 (vs)	1447 (vs)	C–H	
1421 (m)	1419 (m)			N–H (amide III)	[17]
1382 (m)	1384 (m)			N–H	
1319 (m)	1316 (vs)	1317 (vs)	1317 (m)	N–H	
1240 (m)				C–O–C methylester stretching	[17]
1119 (s)	1112 (m)	1108 (vs)	1118 (vs)	C=O stretching	
1070 (vs)				C–OH in-plan bending and stretching	[17]
898 (vw)	875 (w)	875 (s)	875 (vs)	C=O	
781 (m)	781 (s)	781 (vs)	781 (m)	Si–O	
	759 (w)	759 (w)	757 (vw)	C–N	
716 (vw)		713 (vw)	713 (s)	C=O	[19]
666 (vw)	669 (s)	669 (s)	669 (w)	P–OH	[20]
	659 (w)	659 (w)		O=C–N	[21]
620 (w)	619 (m)	617 (m)	619 (s)	Si–O	
		595 (w)		Fe–O	[22]
518 (w)	516 (s)	516 (vs)	516 (m)	P–O	[20]
475 (w)	476 (m)	472 (m)	478 (vs)	N–H	[23]
			420 (m)	Fe–O/Si–O bending	[24,25]

Note: vw: very weak; w: weak; m: medium strong; s: strong; vs: very strong band intensity.

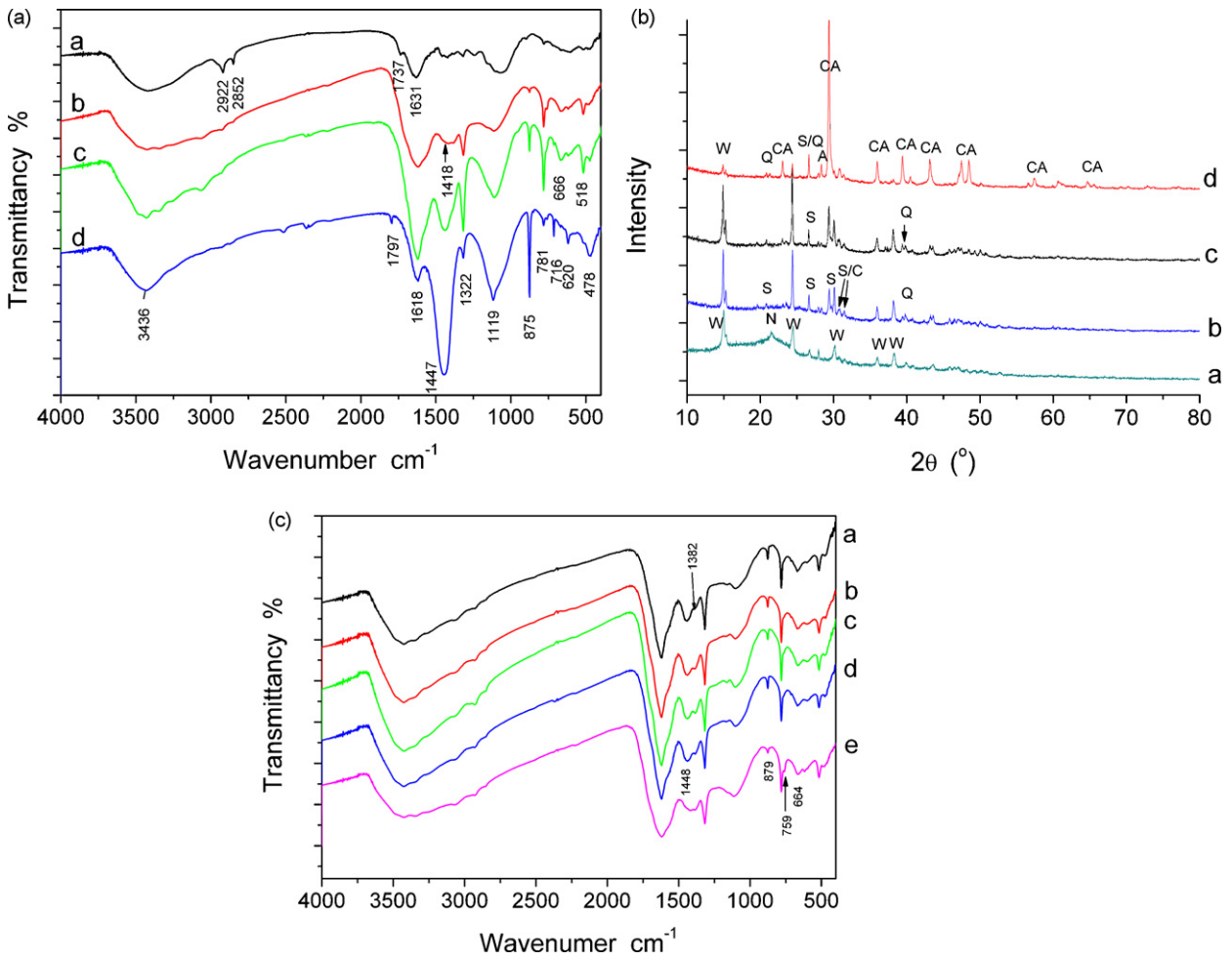

Fig. 1. (a) IR spectra of the adsorbents activated at various temperatures (a: AL1; b: AL2; c: AL3; d: AL4). (b) XRD spectra of crude leaf and activated leaves (a: AL1; b: AL2; c: AL3; d: AL4) (a: albite; ca: calcite; c: calcium phosphate; n: N-pentacosane; q: quartz; s: sodium hydrogen phosphate hydrate; w: whewellite). (c) IR spectra of the Pb(II) loaded and unloaded adsorbent (a: AL2 + Pb1; b: AL2 + Pb2; c: AL2 + Pb3; d: AL2 + Pb4; e: AL2; sorbent dosage: 0.1 g/50 mL; Pb(II) concentration: Pb1 = 10 mg L^{-1}, Pb2 = 20 mg L^{-1}, Pb3 = 40 mg L^{-1}, Pb4 = 80 mg L^{-1}).

groups of AL3 were found similar to those of AL2 based on the IR spectra. The IR pattern of AL4 differed significantly from the other three ALs. The major groups were determined as C=O, CH, and the minor groups were NH, SiO, OH, CN, POH etc. These groups could be ranged as: CH > C=O » NH > OH > SiO > POH > CN according to the relevant band intensity.

The band intensities of CH group at 2922 and 2852 cm^{-1} in AL1 decreased greatly in AL2 and disappeared after activated at higher temperatures. The natural macromolecules (i.e., lignin) contained in the FSL, which remains stable after mulched for 2 months [26], were greatly decomposed in this respect.

Amine was found in all the four adsorbents according to the characteristic bands at wavenumber 1631, 1623 1421, 1382, 1319 and 475 cm^{-1} [23]. The mass percent of N of the foliage may exceed 2% of the dry weight and mostly occurs as enzymes [23,27,28]. The band intensity of NH was found increased with increasing ATs, showing the increased percent of NH group in the ALs.

Calcium oxalate was observed in Fig. 1a due to the reported IR patterns at 1630 and 1330 cm^{-1} [29]. In this study, these bands were found shifted to lower values at 1623 and 1322 cm^{-1}. The intensity of bands relevant to the oxalate in the spectra of AL2 and AL3 was higher than that in the spectra of AL1 and AL4, indicating the higher mass percents of oxalate in AL2 and AL3 than those in AL1 and AL4.

The band at 3415–3426 relevant to OH group become sharper and stronger with increasing ATs, indicating the transformation from organics to inorganics.

To estimate the existence of functional group (C=O), the characteristic peak of C=O should first be affirmed (1650–1800 cm^{-1}). Then the fingerprint peak could be used as assisted proof. The band intensity at 1119 and 875 cm^{-1} was found increased with increasing AT, indicating the increased proportion of the carboxyl group which is a preferential adsorption site for heavy metals [16]. The weak band at 713 cm^{-1} was relevant either to hydrogen bonding with vanadyl group [29] or to carbonate components [19].

In Fig. 1a, the IR bands at 666 and 518 cm^{-1} relevant to phosphate n4 band [20] were strong in spectra of AL2 and AL3, but were very weak in spectra of AL1 and AL4. It was shown that a proper AT (200, 300 °C) was beneficial to preserve the originally contained phosphor element in leaf [30]. After activated at AT ≥ 200 °C, the phosphor (POH) could be transformed into other form, and finally turned to inorganic phosphate (HOP=O) [31].

3.1.2. XRD spectra of various ALs

The XRD patterns of the ALs are shown in Fig. 1b. The increased band intensity and sharpness suggested that a higher AT could produce a higher degree of mineralization of the leaf.

The patterns at 2θ = 14.9, 24.5, 30.2, 36.0 and 38.1° were assigned to whewellite (calcium oxalate hydrate). This compound is insoluble in water and no information suggests that oxalate could adsorb heavy metals. The pattern at 2θ = 24.5° was sharp and strong, indicating that the crystalline of this component was well formed at 300 °C. The intensity of bands associated with whewellite was

increased significantly in spectrum c but decreased greatly in spectrum d compared to spectrum b with respect to the band at $2\theta = 24.5^\circ$.

In spectrum a, only whewellite could be identified as an inorganic component. Although various functional groups had been determined by the IR spectra, only one organic component (normal pentacosane (21.5°)) could be determined. In spectrum b, the broad band at 21.5° was absent, indicating a significantly decreased organic content.

New bands at $2\theta = 20.8$, 26.6, 29.4, 30.1, 30.8 and 31.5° in spectra b and c were assigned to sodium hydrogen phosphate hydrate and calcium phosphate, confirming the observed characteristic bands of phosphate in Fig. 1a. In spectrum d, calcite was found as the most abundant component in AL4. Albite was associated with the band at $2\theta = 28.3^\circ$. Quartz was also observed in all the four spectra indicated by the bands at $2\theta = 20.7$, 26.5, 39.4 and 40.2°, in agreement with the presence of Si–O band in IR spectra as shown in Fig. 1a and Table 2.

3.2. Adsorption isotherms

Fig. 2a shows the isotherms of Pb(II) adsorption on AL1, AL2, AL3 and AL4. The isotherms of AL1 and AL3 are linear type within the concentration range of 1–100 mg L^{-1} while those of AL2 and AL4 are linear when C_e is in the range of 1–10 mg L^{-1}. AL4 showed the best performance in Pb(II) adsorption among the four adsorbents. The affinity of the other three adsorbents towards Pb(II) was sequenced as AL2 > AL1 > AL3.

The adsorption isotherms were fitted with three well-known isothermal models, i.e., Freundlich [32], Langmuir [32] and Dubinin-Radushkevich (D-R) models [33].

The Freundlich model assumes a non-ideal adsorption [32] and can be expressed as:

$$q_e = K_F C_e^{1/n} \quad (1)$$

where K_F and n are the Freundlich constants related to the adsorption capacity and adsorption intensity of the sorbent, respectively.

The Langmuir model assumes a homogeneous monolayer surface sorption and can be written as

$$\frac{1}{q_e} = \frac{1}{Q} + \frac{1}{bQC_e} \quad (2)$$

where Q is the maximum sorption capacity of the adsorbent (mg g^{-1}), and b (L mg^{-1}) the Langmuir constant.

The D-R model assumes a uniform pore-filling sorption and can predict the free sorption energy change by which the sorption type can be judged [33]. The D-R model is written as

$$\ln q_e = \ln q_m - k\varepsilon^2 \quad (3)$$

where q_m is the maximum sorption capacity (mol g^{-1}), k a model constant related to the free sorption energy and ε the Polanyi potential, which is written as

$$\varepsilon = RT \ln\left(1 + \frac{1}{C_e}\right) \quad (4)$$

The mean free energy of sorption (E) is:

$$E = -\frac{1}{\sqrt{2k}} \quad (5)$$

Basically, the adsorption is physical adsorption when $|E|$ is between 1.0 and 8.0 kJ mol^{-1}.

Table 3 shows the predicted model constants. It is found that the Freundlich model could bestfit the isotherms of AL1 and AL3 according to the calculated correlation coefficients (>0.99). The partition coefficients K_F of Pb(II) on AL1 and AL3 were determined at 0.5918 and 0.0594 L g^{-1}, respectively, by Freundlich model. The affinity of the adsorbent towards Pb(II) could be ordered as AL1 > AL3.

As to the isotherms of AL2 and AL4, the correlation coefficients of the test data with Langmuir model ($R^2 > 0.85$) were higher than those with Freundlich and D-R models. The adsorption capacities of Pb(II) on AL2 and AL4 were determined by Langmuir model at 136.7 and 379.3 mg g^{-1}, separately. These values are different from the experimental results. The highest adsorption amount of Pb(II) on AL2 and AL4 was 143.9 and 333.5 mg g^{-1}, respectively.

The maximum adsorption capacity (q_m) predicted by D-R model was in the sequence of AL1 (4.6100 mg g^{-1}) > AL3 (2.0120 mg g^{-1}) > AL4 (0.2631 mg g^{-1}) > AL2 (0.1418 mg g^{-1}). It needs to be noted that the D-R model just describes the amount of adsorbate fixed onto the adsorbent in terms of pore-filling manner. Other researchers have shown similar differences between the adsorption capacity predicted by Langmuir and D-R model [16]. The adsorption capacity predicted by D-R model could not present the real state.

The AL4 has the best performance in Pb(II) adsorption among the four ALs when taking into account of the Pb(II) adsorption capacity (379.3 mg g^{-1}). However, the comparatively low yield efficiency of AL4 (15.26%) limits this positive effect. Instead, AL2 seems to be a better choice for Pb(II) removal from aqueous solution in this study with regard to the satisfying adsorption capacity (132.7 mg g^{-1}) and high yield efficiency (36.52%). Besides, AL2 could be manufactured with a less cost compared to that made at 400 °C because the activation temperature is just half of the latter and this could help to save a lot of energy/power consumption.

The adsorption energy (E) of Pb(II) on various ALs, indicated by D-R model, was in the range of −7.074 to −7.912 kJ mol^{-1} in terms of a physical adsorption. The Freundlich model assumes a multilayered adsorption of solute on the surface of the adsorbent while the D-R model assumes a pore-filling pattern of adsorption. However, further investigations into the surface functional groups and the constituents will help to reveal the adsorption mechanism.

3.3. Effect of adsorbent dosage

Fig. 2b shows the effect of adsorbent dosage on the Pb(II) removal efficiency and the equilibrium Pb(II) concentration. The equilibrium Pb(II) concentration increased from 2.2 to 3.3 mg L^{-1} with increasing adsorbent dosage from 0.025 to 0.05 g/50 mL, and then decreased gradually to 2.1 mg L^{-1} with further increase in adsorbent dosage. The removal efficiency remained larger than 94.84% but less than 96.72%. It was shown that the increase in adsorbent dosage did not obviously give rise to Pb(II) removal efficiency. This phenomenon has been observed in other studies. In dilute slurry the degree of hydration of single sorbent particles is high, thus providing more active sites for heavy metals [34].

3.4. Effect of pH

Fig. 2c shows the variation of Pb(II) adsorption amount and equilibrium pH of solution with initial pH of solution. The q_e and pH_e were found both increased with increasing pH_i. The q_e increased from 1.5 mg g^{-1} rapidly to 30 mg g^{-1} with increasing pH_i from 2.1 to 3.7, and then flattened to reach a maximum at 32.3 mg g^{-1} with further increase in pH_i to 7.6. The pH_es were all higher than pH_i, indicating the high acid-buffering effect of AL. It was beneficial to obtain a higher Pb(II) removal efficiency by keeping the $pH_i > 3.7$. On the other hand, a lower pH could remove the adsorbed Pb(II) from the adsorbent and thus could recycle the adsorbent for repeated utilization.

3.5. Adsorption kinetics

Fig. 2d shows the effect of equilibration time on the amount of adsorbed Pb(II) on AL2. The adsorption equilibrium could be

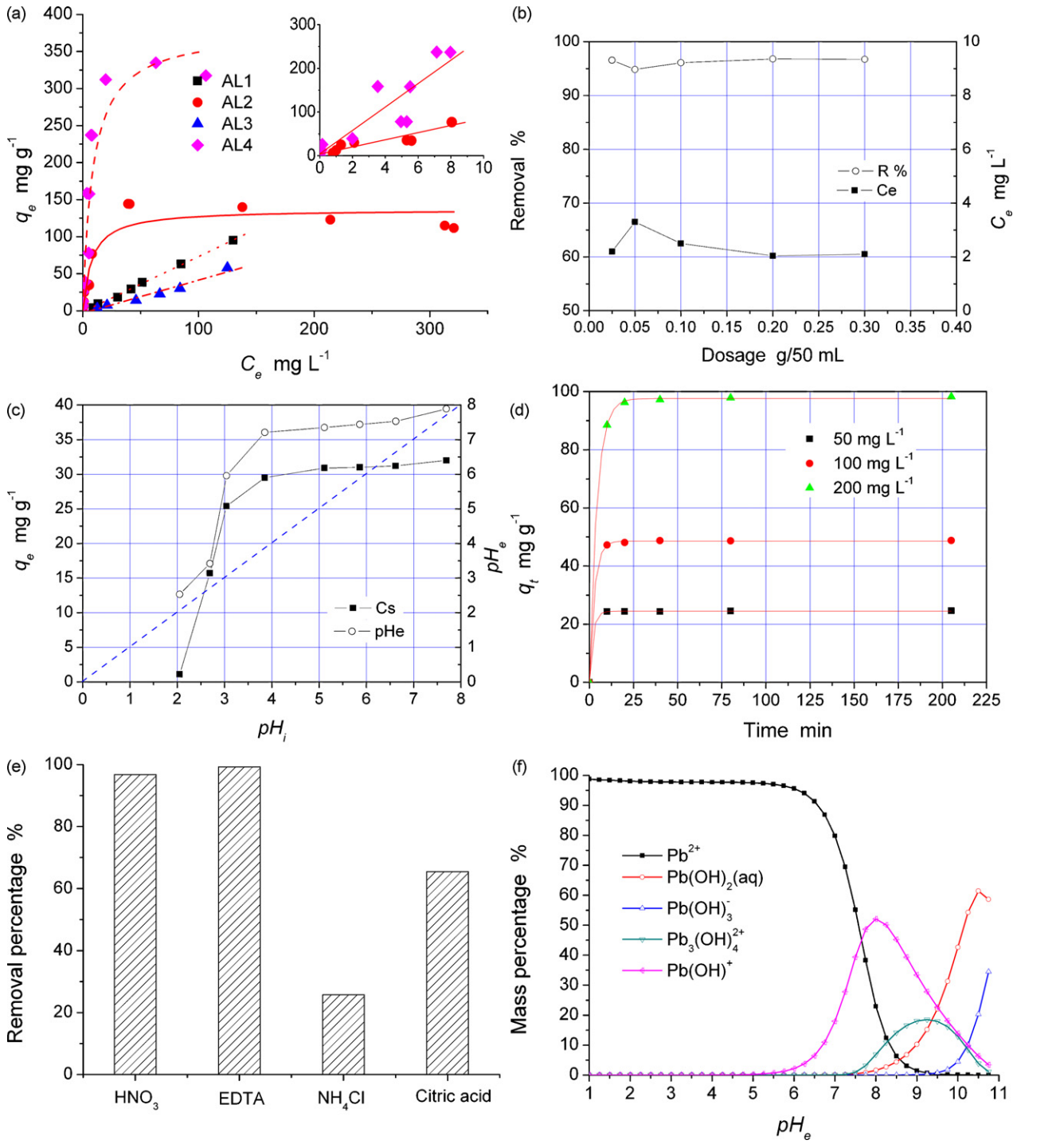

Fig. 2. (a) Adsorption isotherms of Pb(II) adsorption on adsorbents (slurry concentration: 0.1 g/50 mL; 25 °C; 24 h). The inset shows the adsorption isotherms of Pb(II) on AL2 and AL4 as well as the linearly fitted curves at C_e < 10 mg L^{-1}. (b) Effect of adsorbent dosage on Pb(II) removal efficiency and equilibrium Pb(II) concentration (C_0 = 65 mg L^{-1}; 25 °C; 24 h). (c) Effect of pH of solution on equilibrium adsorption amount (C_0 = 65 mg L^{-1}; 0.1 g/50 mL; 25 °C). (d) Effect of reaction time on the amount of Pb(II) adsorption on AL2 (lines were fitted by Pseudo-first order kinetics using nonlinear least square regression method; test conditions: 25 °C, 180 rpm, 0.1 g/50 mL). (e) Effect of various agents on Pb(II) removal percentage from AL2. (f) Species distribution of Pb(II) in solution with pH$_e$ (Pb(II): 50 mg L^{-1}; NO_3^-: 100 mg L^{-1}; ionic strength: 0.001 M).

Table 3
Predicted isothermal model constants for Pb(II) adsorption on various ALs.

Sample no.	Freundlich isotherm			Langmuir isotherm			D-R isotherm			
	K_F (L g^{-1})	$1/n$	R^2	Q (mg g^{-1})	b (L mg^{-1})	R^2	q_m (mg g^{-1})	k	E (kJ mol^{-1})	R^2
AL1	0.5918	1.0454	0.9972	NA	NA	NA	4.6100	9.73E-09	−7.168	0.9757
AL2	41.73	0.1882	0.6729	136.7	0.1299	0.9058	0.1418	1.327E-08	−7.074	0.8786
AL3	0.0594	1.4219	0.9916	NA	NA	NA	2.0120	9.55E-09	−7.236	0.9879
AL4	79.36	0.3340	0.7719	379.3	0.1155	0.8579	0.2631	7.871E-09	−7.912	0.8176

achieved within 20 min. The test data was further analyzed with three kinetic models (i.e., Pseudo-first order kinetics, Pseudo-second order kinetics and intraparticle diffusion model) [35].

The Pseudo-first order kinetics could be shown as:

$$\log(q_e - q) = \frac{\log q_e - k_1 t}{2.303} \quad (6)$$

where q (mg g^{-1}) is the amount of solute adsorbed per gram of adsorbent over a time period t (min), q_e (mg g^{-1}) the equilibrium adsorption amount and k_1 (min^{-1}) the first-order kinetic constant.

The Pseudo-second order kinetics are expressed as

$$\frac{t}{q} = \frac{1}{k_2 q_e^2} + \frac{t}{q_e} \quad (7)$$

where k_2 (g mg^{-1} min^{-1}) is the kinetic constant.

The intraparticle diffusion model is based on the transfer of matter from the external surface to the internal surface inside of the pores, and is expressed as:

$$q = K_D t^{1/2} \quad (8)$$

where K_D (g mg^{-1} min^{-1}) is the constant of intraparticle diffusion.

Table 4 shows the predicted model constants for the three kinetic models. Both of the Pseudo-first and the Pseudo-second order kinetics could well-fit the test data with correlation coefficients higher than 0.9999. The predicted equilibrium adsorption capacities (q_e) by Pseudo-first order kinetics were 24.48, 48.60 and 97.63 mg g^{-1}, separately for solutions with initial Pb(II) concentrations at 50, 100 and 200 mg L^{-1}. The predicted constants q_e by the Pseudo-second order kinetics were 24.66, 48.85 and 98.62 mg g^{-1}, separately for solutions at C_0 50, 100 and 200 mg L^{-1}. The kinetic model constants k_1 were determined at 0.5190, 0.3577 and 0.2361, while the k_2 were 0.1399, 0.0812 and 0.01397, separately at C_0 50, 100 and 200 mg L^{-1}. The equilibrium adsorption amount (q_e) increased with increasing solute concentration, while the adsorption rate (k_1 and k_2) decreased with increasing solute concentration. However, the adsorption rapidly reached the equilibrium within 20 min for solutions with different C_0 as shown in Fig. 2d.

The intraparticle diffusion model was found unsuitable to fit the kinetic test data in terms of the correlation coefficient in spite of the high correlation (0.9469) at C_0 50 mg L^{-1}. Associated with the large average pore size of AL2 (617.3 Å), the adsorption might not be dominated by the intraparticle diffusion process. A surface adsorption could be speculated by the kinetic study, different from the pore-filling manner of adsorption indicated by analysing the isotherms with D-R model.

3.6. Recycling of waste adsorbent

Fig. 2e shows the effect of various agents on the removal percent of Pb(II) from waste AL2. The R % of Pb(II) from the waste AL2 was determined at 99.3, 96.8, 65.5 and 25.7, respectively, when recycled using 0.01 M EDTA, HNO_3, citric acid and NH_4Cl solution. As a strong chelating agent, EDTA could effectively remove heavy metals from various adsorbents [16]. In this study, the performance of EDTA was found to be the best of all. Besides, the effect of 0.01 M nitric acid on Pb(II) removal was also satisfying. When taking account of the cost efficiency, the nitric acid seems a better choice. In this respect, the adsorbent could be repeatedly used in the treatment of Pb(II) polluted wastewaters.

3.7. Discussion of adsorption mechanism

3.7.1. Species distribution of Pb(II) in aqueous solution

The species distribution of Pb(II) in aqueous solution was calculated using Visual MINTEQ v2.53 based on the MINTEQA2 thermodynamic database. The parameters were set as: lead nitrate $Pb(NO_3)_2$ (50 mg L^{-1}), 0.001 M background ionic strength, $1 < pH_e < 12$, 1 atm and 25 °C. The percentage of the ionic species of Pb(II) at various pHs was shown in Fig. 2f. The species of Pb(II) is mainly Pb^{2+} (>98%) at pH < 6.0, followed by a sharp reduction in Pb^{2+} at 6.0 < pH < 9.0. Lead hydroxyl complexes in the form of $Pb(OH)^+$, $Pb_4(OH)_4{}^{4+}$ and $Pb_3(OH)_4{}^{2+}$ are formed at pH > 6.0, whereas the $Pb(OH)^+$ reaches the peak (52.04%) at pH 8.0 and the $Pb_3(OH)_4{}^{2+}$ shows slow increase at pH > 7.5 and reaches its peak (18.52%) at pH 9.25. The precipitation of lead is in the form of $Pb(OH)_2$ at pH > 8.0 and the maximum is 61.43% at pH 10.5.

3.7.2. FT-IR patterns analysis

Fig. 1c shows the FT-IR spectra of AL2 with and without Pb(II) loadings. Increased concentration of Pb(II) was equilibrated with the adsorbent AL2 to investigate the relevant functional groups relevant to the Pb(II) adsorption. The characteristic IR band could be assigned to specific functional group as shown in Table 2.

The bands at 1419, 1384, 1316, 759 and 476 cm^{-1} could be assigned to the vibration of –CNH group. The band at 1419 in AL2 was found shifted to 1448 with increased band intensity after Pb(II) adsorption, confirming the interaction existed between the CNH group and Pb(II) [36]. Amine group was reported as a significant binding site for metal uptake in biosorbents [30]. As an alkaline functional group, amine could give rise to the solution pH. This property has been utilized in CO_2 capture techniques [37]. In this study, the equilibrium pH of the adsorbent/water slurry (1/10) was higher than 9.10, corresponding to the presence of alkaline component in AL2. The high affinity of amine towards Pb(II) along with the increased solute pHe would contribute to the adsorption of Pb(II) on AL2. However, the deprotonated amine group would turn to possess positive charges at pH < 2.0. This behavior might pronouncedly reduce the Pb(II) adsorption capacity, which could explain the sharp edge observed in Fig. 2c. Based on the theoretically calculated species distribution of Pb(II) as shown in Fig. 2f, the reversible reaction of Pb(II) with the amine group could be shown as:

$$R\text{–}CNH_2 + Pb(OH)^+ \rightleftharpoons R\text{–}CNHPb(OH) + H^+ \quad (9)$$

$$R\text{–}CNH_2 + Pb^{2+} \rightleftharpoons R\text{–}CNHPb^+ + H^+ \quad (10)$$

On the other hand, the presence of phosphate (at wavenumber 669 and 516 cm^{-1}) would contribute to the adsorption of Pb(II) in the form of

$$MHPO_4 + Pb^{2+} \rightarrow PbHPO_4(s) + M^{2+} \quad (11)$$

in terms that the component of $MHPO_4$ in the adsorbent was soluble. If the cation M was calcium or magnesium, the above reaction

Table 4
Predicted kinetic constants for Pb(II) adsorption on AL2.

C_0 (mg L^{-1})	Pseudo-first order kinetics			Pseudo-second order kinetics			Intraparticle diffusion kinetics		
	q_e (mg g^{-1})	k_1 (min^{-1})	R	q_e (mg g^{-1})	k_2 (g mg^{-1} min^{-1})	R	C (mg g^{-1})	k_{int} (mg g^{-1} min$^{-1/2}$)	R
50	24.48	0.5190	0.9999	24.66	0.1399	1.000	24.26	0.02696	0.9469
100	48.60	0.3577	0.9999	48.85	0.0812	1.000	47.51	0.1081	0.7308
200	97.63	0.2361	0.9999	98.62	0.01397	0.9999	91.02	0.6160	0.6728

Table 5
Reported adsorption capacity of Pb(II) on various adsorbents.

Materials	Predicted adsorption capacity ($mg\,g^{-1}$)	Reference
Brown seaweed	252.0	[4]
Pecan nutshell	195.8	[5]
Green algae Spirogyra	140.0	[6]
Distillery sludge	51.0	[7]
Tobacco dust	39.6	[8]
Macroalga *Caulerpa lentillifera*	29.4	[9]
Olive stone waste	9.25	[10]
Firmiana Simplex leaf (AL2)	132.7	This study
Firmiana Simplex leaf (AL4)	379.3	This study

will become insignificant with respect to its comparatively low dissolution coefficients.

The strong band at $879\,cm^{-1}$ in the IR spectrum of AL4 was assigned to Type A carbonate (carbonate ions occupying monovalent OH sites in the apatitic structure) [38], corresponding to the high calcite content identified by the XRD spectra. Because calcite could effectively remove heavy metals from solutions [16], the best performance of AL4 in all the four Als to remove Pb(II) could be primarily attributed to the abundant calcite composition. Besides, the natural pH_{na} of AL4 (10.92) must be relevant to the formed calcite. As a result, the sorption of Pb(II) on AL4 may be written as:

$$CaCO_3 + Pb^{2+} \rightarrow PbCO_3(s) + Ca^{2+} \quad (12)$$

This is a chemical sorption and could be linked to the results of D-R analysis (the least adsorption energy ($-7.912\,kJ\,mol^{-1}$) indicates the presence of chemical adsorption).

However, as to AL2, the intensity of the band relevant to carbonate had no obvious change after Pb(II) adsorption even with increasing Pb(II) loading (up to $40\,mg\,g^{-1}$), indicating that the carbonate contained in AL2 was not the dominant adsorption site for Pb(II).

Accordingly, the difference in Pb(II) adsorption capacity of the ALs might be caused by:

(i) increased phosphate and amine content leads to an increased adsorption capacity of AL2;
(ii) high percentage of whewellite decreases the adsorption capacity of AL3;
(iii) significantly increased calcite content makes AL4 the most preferential adsorbent for Pb(II).

Correlating with the surface property of each AL, the average pore size (sequenced as AL4 > AL2 ≫ AL3) was found directly related to the adsorption capacity. Although AL4 shows the best performance, AL2 has a much higher yield efficiency and a moderately high adsorption affinity towards Pb(II), which make it to be a better choice.

Various biosorbents have been investigated with respect to Pb(II) adsorption performance. Table 5 shows the Pb(II) adsorption capacities of some recently reported biosorbents. The activated Firmiana Simplex leaf (AL4) has the highest Pb(II) adsorption capacity among the reported adsorbents. Different and superior to other biosorbents, the ALs developed in this study are partly decomposed into inorganics which are stable in the environment and are able to be recycled for further usage. Besides, the other sorbents are rare in China. As a widely planted tree, the Firmiana Simplex provides a locally available cheap source of adsorbent. The activation method provided here proves effective and appears promising in the treatment of heavy metals contained wastewaters.

4. Conclusions

(1) After activation, the mass percent of inorganic components (including whewellite, quartz, phosphate and calcite) increased and the specific surface area increased from 0.08283 to $9.32\,m^2\,g^{-1}$ with the increasing activation temperature (AT) from 100 to 400 °C. Proper activation temperature (200 °C) helps to preserve the amine and carboxyl groups which are beneficial to Pb(II) adsorption.
(2) The adsorption isotherms of Pb(II) on AL1 and AL3 were best-fitted by Freundlich model while those on AL2 and AL4 were bestfitted by Langmuir model. The affinities of the adsorbents towards Pb(II) were sequenced as AL4 > AL2 > AL1 > AL3.
(3) The adsorbent activated at 200 °C was found most suitable for Pb(II) adsorption regarding the high yield efficiency (36.52%), high Pb(II) adsorption capacity ($136.7\,mg\,g^{-1}$ by Langmuir model), high adsorption affinity (H type isotherm) and rapid adsorption rate (within 20 min by kinetic study).
(4) The Pb(II) removal efficiency of AL2 was obviously affected by the solution pH rather than by the adsorbent dosage. The IR pattern analysis indicates that the adsorption of Pb(II) on AL2 is a chemical process involving the complexation with amine groups and the ion exchange with phosphate. The average pore size of the adsorbent was found directly related to the adsorption capacity.
(5) The activation method proposed in this paper was proved effective and potentially applicable in the treatment of Pb(II) polluted wastewaters.

Acknowledgements

The authors would like to express their sincere gratitude to the Key Project of National Natural Science Foundation of China (NSFC) (Grant 50538080) and National Science Fund for Distinguished Young Scholars (Grant 50425825) for the financial support to this study.

References

[1] WHO, Guidelines for Drinking-water Quality: Incorporating First Addendum, vol. 1, Recommendations, third ed., World Health Organisation, Geneva, 2006.
[2] Y.M. Han, P.X. Du, J. Cao, E.S. Posmentier, Multivariate analysis of heavy metal contamination in urban dusts of Xi'an, Central China, Sci. Total Environ. 355 (1–3) (2006) 176–186.
[3] X.Y. Bi, X.B. Feng, Y.G. Yang, Environmental contamination of heavy metals from zinc smelting areas in Hezhang County, western Guizhou, China, Environ. Int. 32 (7) (2006) 883–890.
[4] M.T.K. Tsui, K.C. Cheung, N.F.Y. Tam, M.H. Wong, A comparative study on metal sorption by brown seaweed, Chemosphere 65 (1) (2006) 51–57.
[5] C.P. Julio et al., Pecan nutshell as biosorbent to remove Cu(II), Mn(II) and Pb(II)from aqueous solutions, J. Hazard. Mater. 162 (1) (2009) 270–280.
[6] V.K. Gupta, A. Rastogi, Biosorption of lead from aqueous solutions by green algae Spirogyra species: kinetics and equilibrium studies, J. Hazard. Mater. 152 (1) (2008) 407–414.
[7] R. Nadeem, M.A. Hanif, F. Shaheen, S. Perveen, M.N. Zafar, T. Iqbal, Physical and chemical modification of distillery sludge for Pb(II) biosorption, J. Hazard. Mater. 150 (2) (2008) 335–342.
[8] B.C. Qi, C. Aldrich, Biosorption of heavy metals from aqueous solutions with tobacco dust, Bioresource Technol. 99 (2008) 5595–5601.
[9] R. Apiratikul, P. Pavasant, Batch and column studies of biosorption of heavy metals by *Caulerpa lentillifera*, Bioresource Technol. 99 (8) (2008) 2766–2777.
[10] N. Fiol, I. Villaescusa, M. Martinez, N. Miralles, J. Poch, J. Serarols, Sorption of Pb(II), Ni(II), Cu(II) and Cd(II) from aqueous solution by olive stone waste, Sep. Purif. Technol. 50 (2006) 132–140.
[11] S.S. Ahluwalia, D. Goyal, Removal of heavy metals by waste tea leaves from aqueous solution, Eng. Life Sci. 5 (2005) 158–162.
[12] Ontario Ministry of the Environment, Environmental Risks of Municipal Non-hazardous Waste Landfilling and Incineration, Queen's Printer for Ontario, 1999.
[13] M.A.K.M. Hanafiah, W.S.W. Ngah, H. Zakaria, S.C. Ibrahim, Batch study of liquid-phase adsorption of lead ions using lalang (*Imperata cylindrica*) leaf powder, J. Biol. Sci. 7 (2007) 222–230.
[14] R.P. Han, W.H. Zou, W.H. Yu, S.J. Cheng, Y.F. Wang, J. Shi, Biosorption of methylene blue from aqueous solution by fallen phoenix tree's leaves, J. Hazard. Mater. 141 (2007) 156–162.

[15] K. Ranganathan, Chromium removal by activated carbons prepared from *Casurina equisetifolia* leaves, Bioresource Technol. 73 (2000) 99–103.
[16] X.W. Tang, Z.Z. Li, Y.M. Chen, Y. Wang, Removal of Cu(II) from aqueous solution by adsorption on Chinese Quaternary Loess: kinetics and equilibrium studies, J. Environ. Sci. Health A 43 (2008) 779–791.
[17] A. Sinitsya, J. Copıkova, V. Prutyanov, S. Skoblya, V. Machovic, Amidation of highly methoxylated citrus pectin with primary amines, Carbohydr. Polym. 42 (2000) 359–368.
[18] A. John, D. Philip, K.R. Morgan, S. Devanarayanan, IR and Raman spectra of two layered aluminium phosphates Co(en)3$Al_3P_4O_{16}$·3H_2O and $[NH_4]_3[Co(NH_3)_6]_3[Al_2(PO_4)_4]_2$·2$H_2O$, Spectrochim. Acta A 56 (2000) 2715–2723.
[19] K.D.O. Jackson, A guide to identifying common inorganic fillers and activators using vibrational spectroscopy, Internet J. Vib. Spectrosc. 2 (1998), http://www.ijvs.com/volume2/edition3/section3.html#jackson.
[20] J. Salas, Z. Benzo, G. González, Synthesis of hydroxyapatite by mechanochemical transformation, Rev. Lat. Am. Met. Mat. 24 (2004) 12–16.
[21] M.M.E. Jacob, A.K. Arof, FTIR studies of DMF plasticized polyvinyledene fluoride based polymer electrolytes, Electrochim. Acta 45 (2000) 1701–1706.
[22] S. Ram, Infrared study of the dynamics of boroxol rings in the crystallization of $BaFe_{12}O_{19}$ microcrystals in borate glasses, Phys. Rev. B 51 (1995) 6280–6286.
[23] R.A. Jones, Pyrrole studies. I. The infrared spectra of 2-monosubstituted pyrroles, Aust. J. Chem. 16 (1963) 93–100.
[24] J. Chorover, M.K. Amistadi, O.A. Chadwick, Surface charge evolution of mineral-organic complexes during pedogenesis in Hawaiian basalt, Geochim. Cosmochim. Acta 68 (2004) 4859–4876.
[25] K. Ramaswamy, M. Kamalakkannan, Infrared study of influence of temperature on clay minerals, J. Therm. Anal. Calorim. 44 (1995) 1388–6150.
[26] Z. Jin, T. Akiyama, B.Y. Chung, Y. Matsumoto, K. Iiyama, S. Watanabe, Changes in lignin content of leaf litters during mulching, Phytochemistry 64 (2003) 1023–1031.
[27] S.G. Pallardy, Nitrogen Metabolism, Physiology of Woody Plants, third ed., Elsevier Inc., 2008, pp. 233–254.
[28] M.A. Moharram, A. Higazi, A.A. Moharram, Infrared spectra of urine from cancerous bladders, Int. J. Infrared Millim. Wave 17 (1996) 1572–9559.
[29] Y. Repelin, E. Husson, L. Abello, G. Lucazeau, Structural study of gels of V_2O_5: normal coordinate analysis, Spectrochim. Acta A 41 (1985) 993–1003.
[30] M. Kılıç, M.E. Keskin, S. Mazlum, N. Mazlum, Hg(II) and Pb(II) adsorption on activated sludge biomass: effective biosorption mechanism, Int. J. Mineral Process. 87 (2008) 1–8.
[31] A. Salvà, J. Frau, F. Muñoz, B. Vilanova, J. Donoso, FT-IR study of pyridoxamine 5′phosphate, Biochim. Biophys. Acta 1647 (2003) 83–87.
[32] D.D. Do, Adsorption Analysis: Equilibria and Kinetics, Imperial College Press, London, 1998.
[33] J. Romero-Gonzalez, J.R. Peralta-Videa, E. Rodrıguez, S.L. Ramirez, J.L. Gardea-Torresdey, Determination of thermodynamic parameters of Cr(VI) adsorption from aqueous solution onto *Agave lechuguilla* biomass, J. Chem. Thermodyn. 37 (2005) 343–347.
[34] X.W. Tang, Z.Z. Li, Y.M. Chen, Behaviour and mechanism of Zn(II) adsorption on Chinese loess at dilute slurry concentrations, J. Chem. Technol. Biotechnol. 83 (5) (2008) 673–682.
[35] Y.S. Ho, G. McKay, A comparison of chemisorption kinetic models applied to pollutant removal on various sorbents, Trans. Inst. Chem. Eng. 76B (1998) 332–340.
[36] M. Barbaro, R.H. Urbina, C. Cozza, D. Fuerstenau, A. Marabini, Flotation of oxidized minerals of copper using a new synthetic chelating reagent as collector, Int. J. Mineral Process. 50 (1997) 275–287.
[37] M.L. Gray, Y. Soong, K.J. Champagne, J. Baltrus, R.W. Stevens, P. Tochinda, S.S.C. Chuang, CO_2 capture by amine-enriched fly ash carbon sorbents, Sep. Purif. Technol. 35 (2004) 31–36.
[38] N. Vyavahare, M. Ogle, F.J. Schoen, R.J. Levy, Elastin calcification and its prevention with aluminum chloride pretreatment, Am. J. Pathol. 155 (1999) 973–982.